

3-D SPH Simulations of Colliding Winds in η Carinae

Atsuo T. Okazaki¹, Stanley P. Owocki², Christopher M. P. Russell³
and Michael F. Corcoran⁴

¹Faculty of Engineering, Hokkai-Gakuen University, Toyohira-ku, Sapporo 062-8605, Japan
email: okazaki@elsa.hokkai-s-u.ac.jp

²Bartol Research Institute, University of Delaware, Newark, 19716 DE, USA
email: owocki@bartol.udel.edu

³Department of Physics and Astronomy, University of Delaware, Newark, 19716 DE, USA
email: crussell@udel.edu

⁴Universities Space Research Association, Goddard Space Flight Center,
Greenbelt, MD 20771, USA
email: corcoran@milkyway.gsfc.nasa.gov

Abstract. We study colliding winds in the superluminous binary η Carinae by performing three-dimensional, Smoothed Particle Hydrodynamics (SPH) simulations. For simplicity, we assume both winds to be isothermal. We also assume that wind particles coast without any net external forces. We find that the lower density, faster wind from the secondary carves out a spiral cavity in the higher density, slower wind from the primary. Because of the phase-dependent orbital motion, the cavity is very thin on the periastron side, whereas it occupies a large volume on the apastron side. The model X-ray light curve using the simulated density structure fits very well with the observed light curve for a viewing angle of $i = 54^\circ$ and $\phi = 36^\circ$, where i is the inclination angle and ϕ is the azimuth from apastron.

Keywords. stars: individual (η Car) – stars: winds, outflows – hydrodynamics – methods: numerical – binaries: general

1. Introduction

η Carinae is one of the most luminous and massive stars in the Galaxy. It has exhibited a series of mass ejection episodes, the most notable of which was the Great eruption in the 1840's when the star ejected mass of $\sim 10 M_\odot$, from which the Homunculus nebula was formed. Its current mass and luminosity are $M \sim 10^2 M_\odot$ and $L \sim 5 \times 10^6 L_\odot$, respectively.

The spectrum of η Car is rich in emission lines and has no photospheric lines. Daminieli (1996) first noticed a 5.5 yr periodicity in the variability of the He I 10830Å line. Later, other optical lines were also found to show variations with the same periodicity. In the X-ray band, the flux exhibits particularly interesting, periodic variability: After a gradual increase toward periastron, the X-ray flux suddenly drops to a minimum, which lasts for about three months. It then recovers to a level slightly higher than that at apastron (Ishibashi *et al.* 1999; Corcoran 2005; see also Fig. 3). All these variations are consistent with the system being a long-period ($P_{\text{orb}} = 2,024$ days), highly eccentric ($e \sim 0.9$) binary. The X-ray emission is considered to arise from the wind collision region.

Although there is mounting evidence that η Car is a supermassive binary, it is very hard to directly observe the stars. They are buried deep inside dense winds, which are further engulfed by the optically thick, Homunculus nebula. As a result, even the viewing angle

Table 1. Stellar, wind, and orbital parameters

Parameters	η Car A	η Car B
Mass (M_{\odot})	90	30
Radius (R_{\odot})	90	30
Mass loss rate ($M_{\odot} \text{ yr}^{-1}$)	2.5×10^{-4}	10^{-5}
Wind velocity (km s^{-1})	500	3,000
Wind temperature (K)	3.5×10^4	3.5×10^4
Orbital period P_{orb} (d)	2,024	
Orbital eccentricity e	0.9	
Semi-major axis a (cm)	2.3×10^{14}	

is not well constrained. It is therefore important to construct a 3-D dynamical model, on the basis of which the observed features are interpreted.

In this paper, we give a brief summary of the results from 3-D numerical simulations of colliding winds in η Car. Detailed results will be published elsewhere (Okazaki *et al.* 2008).

2. Numerical Model

Simulations presented here were performed with a 3-D Smoothed Particle Hydrodynamics (SPH) code. The code is based on a version originally developed by Benz (Benz 1990; Benz *et al.* 1990) and then by Bate and his collaborators (Bate, Bonnell & Price 1995). It uses the variable smoothing length, and the SPH equations with the standard cubic-spline kernel are integrated with individual time steps for each particle. In our code, the winds are modeled by an ensemble of gas particles, which are continuously ejected with a given outward velocity at a radius just outside each star. The artificial viscosity parameters adopted are $\alpha_{\text{SPH}} = 1$ and $\beta_{\text{SPH}} = 2$.

For simplicity, we take both winds to be isothermal and coasting without any net external forces, assuming in effect that gravitational forces are canceled by radiative driving terms. We set the binary orbit on the x - y plane and the major axis of the orbit along the x -axis (the apastron is in the $+x$ -direction). The outer simulation boundary is set at either $r = 10.5a$ or $r = 105a$ from the centre of mass of the system, where a is the semi-major axis of the binary orbit. Particles crossing this boundary are removed from the simulation. In the following, $t = 0$ (Phase 0) corresponds to the periastron passage.

Table 1 summarizes the stellar, wind, and orbital parameters adopted in our simulations. With these parameters, the ratio η of the momentum fluxes of the winds from η Car A and B is $\eta \sim 4.2$. The parameters adopted here are consistent with those derived from observations (Corcoran *et al.* 2001; Hillier *et al.* 2001), except for the wind temperature of η Car A. As mentioned above, we take the same temperature for both winds for simplicity. Note that the effect of wind temperature on the dynamics of high-velocity wind collision is negligible.

3. Structure and evolution of colliding winds

Figure 1 shows the wind collision interface geometry at $t \sim 0$ (at periastron; top panel), $t \sim 50$ d (during the X-ray minimum; middle panel), and $t \sim 200$ d (after the X-ray minimum; bottom panel) in a simulation covering $r \leq 10.5a$. In each panel, the greyscale plot shows the density in the orbital plane (left panel) and the plane perpendicular to the

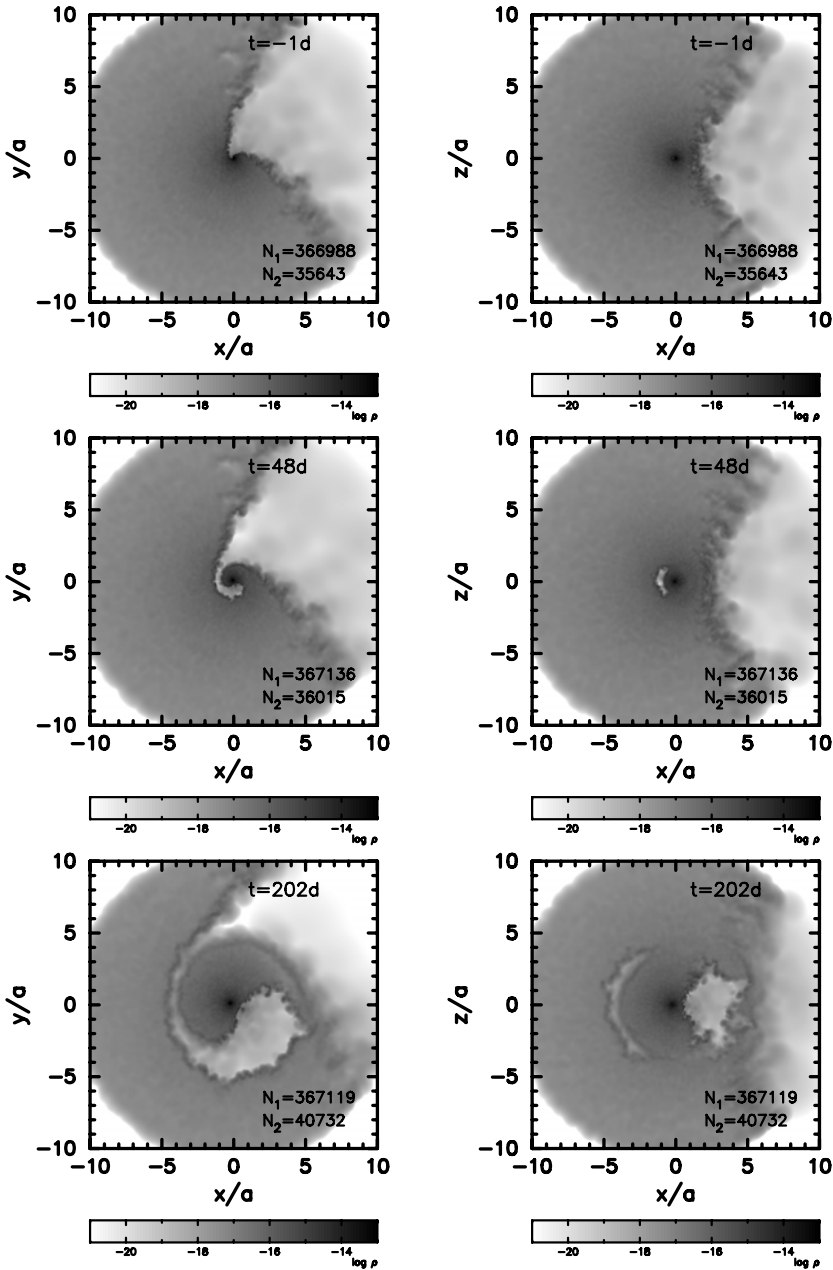


Figure 1. Wind collision interface geometry at $t \sim 0$ (top), $t \sim 50$ d (middle), and $t \sim 200$ d (bottom) for $r \leq 10a$. In each panel, the greyscale plot shows the density in the orbital plane (left) and the plane which is perpendicular to the orbital plane and through the major axis of the orbit (right), on a logarithmic scale with cgs units. The dark spot near the origin represents the primary, while the small dark spot close to the apex of the lower density wind represents the secondary. Annotations in each panel give the time (in days) from periastron passage and the numbers of particles in the primary wind, N_1 , and in the secondary wind, N_2 .

orbital plane and through the major axis of the orbit (right panel), on a logarithmic scale with cgs units. The dark spot near the origin represents the primary (η Car A), while

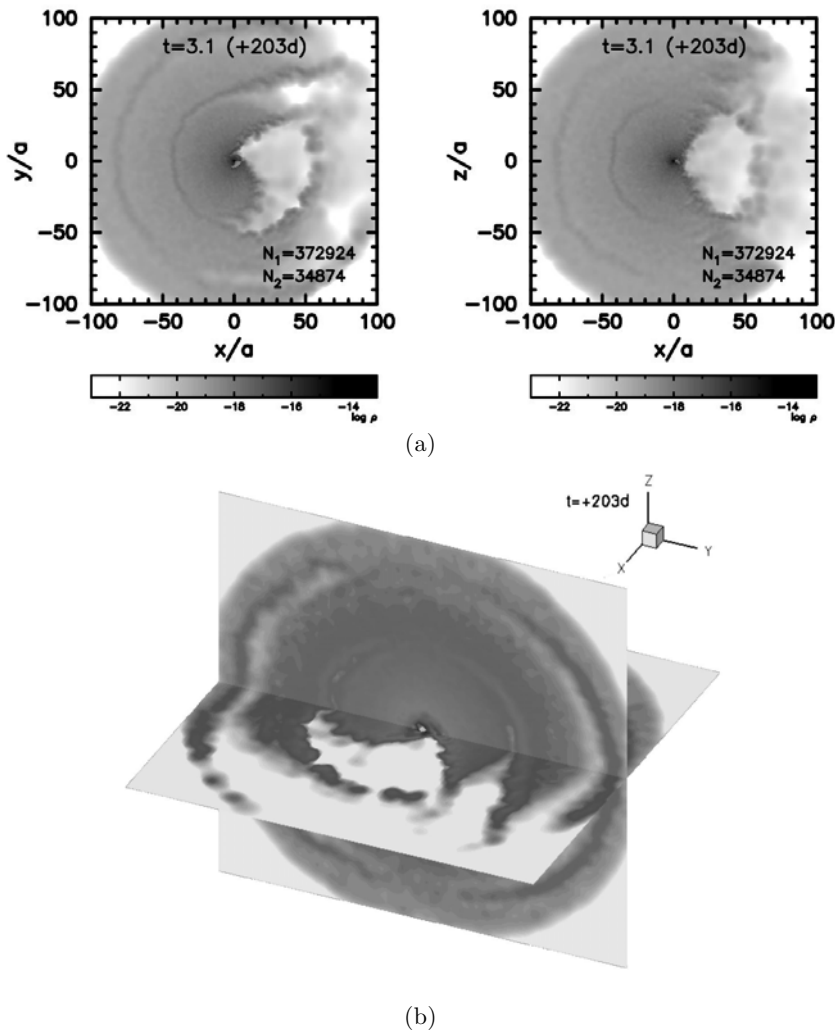


Figure 2. Wind collision interface geometry at $t \sim 200$ d within $r = 100a$: (a) 2-D density maps in the orbital plane (left) and the plane perpendicular to the orbital plane and through the major axis of the orbit (right) and (b) the 3-D plot of the logarithmic density.

the small dark spot close to the apex of the lower density wind represents the secondary (η Car B).

Although the wind collision interface in the simulation exhibits variations from instabilities, its global shape is easily traced and illustrates how the lower density, faster wind from the secondary makes a cavity in the higher density, slower wind from the primary. As expected, the shape of the collision interface around apastron, where the orbital speed of the secondary is only $\sim 20 \text{ km s}^{-1}$ with respect to the primary, is in agreement with the analytical one (e.g., Antokhin *et al.* 2004). As the secondary approaches the periastron, the interface begins to bend, and at phases around periastron, where the orbital speed of the secondary is $\sim 360 \text{ km s}^{-1}$ with respect to the primary, the lower density wind from the secondary makes a thin layer of cavity along the orbit. Then, the thickness of the cavity increases as the secondary moves away from periastron.

In order to study the wind collision interface geometry on a larger scale, we have performed a simulation covering $r \leq 105a$. Figure 2(a) shows the 2-D density maps in

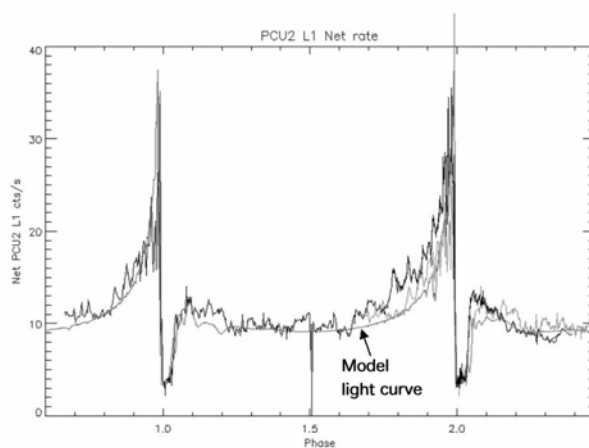


Figure 3. Comparison of RXTE data (black and gray lines; see Corcoran 2005) with the closest match model light curve (less-jaggy gray line). The light gray line shows the first cycle of RXTE data shifted by one period. Taken from Russell *et al.* (this volume).

the orbital plane and the plane perpendicular to it at the same phase (Phase 0.1) as that of the bottom panel of Fig. 1. The 3-D interface geometry is shown in Fig. 2(b) by the logarithmic density plot. From Fig. 2, we note that the lower density wind from the secondary carves out a large-scale, spiral cavity in the higher density wind from the primary. The shape of the cavity is very asymmetric. It is just a thin layer on the periastron side with respect to the primary, whereas it occupies a large volume on the apastron side.

It is interesting to study whether the model presented here can explain the variability in the RXTE X-ray light curve. Using the density distribution in our $r = 10a$ simulation, Russell *et al.* (this volume) modeled the X-ray light curve and compared it with the observed light curve. Assuming that the X-ray emission occurs at the head of the wind-wind interaction cone located at $D/(1 + \sqrt{\eta})$ from the secondary, where D is the binary separation, and varies in intensity with D^{-1} at any given orbital phase, they generated trial X-ray light curves by computing the phase variation of absorption to observers at various assumed lines of sight. They found that the RXTE X-ray light curve is very well fit with an optimal viewing angle of approximately 54 degrees of inclination and 36 degrees from apastron in the prograde direction (see Fig. 3 from Russell *et al.* (this volume) for the comparison between the model and observed X-ray light curves). The excellent fit seen in Fig. 3 confirms that the current model basically gives a correct picture of the wind-wind collision interaction in η Carinae.

4. Conclusions

We have studied the wind collision interaction in the supermassive binary η Carinae, carrying out 3-D SPH simulations. The results from simulations have clarified how the lower density, faster wind from the secondary (η Car B) carves out a cavity in the higher density, slower wind from the primary (η Car A). With an optimal viewing angle of $i = 54^\circ$ and $\phi = 36^\circ$, where i is the inclination angle and ϕ is the azimuth measured from apastron in the prograde direction, the model gives an excellent fit with the RXTE X-ray light curve (Russell *et al.* this volume).

Acknowledgements

A.T.O. thanks Japan Society for the Promotion of Science for the financial support via Grant-in-Aid for Scientific Research (16540218). SPH simulations were performed on HITACHI SR11000 at Hokkaido University Information Initiative Center.

References

- Antokhin, I. I., Owocki, S. P., & Brown, J. C. 2004, *ApJ*, 611, 434
 Bate, M. R., Bonnell, I. A., & Price, N. M. 1995, *MNRAS*, 285, 33
 Benz, W. 1990, in: J. R. Buchler (ed.), *The Numerical Modelling of Nonlinear Stellar Pulsations* (Dordrecht: Kluwer), p. 269
 Benz, W., Bowers, R. L., Cameron, A. G. W., & Press, W. H. 1990, *ApJ*, 348, 647
 Corcoran, M. F., Ishibashi, K., Swank, J. H., & Petre, R. 2001, *ApJ*, 547, 1034
 Corcoran, M. F. 2005, *AJ*, 129, 2018
 Daminieli, A. 1996, *ApJ*, 460, L49
 Hillier, D. J., Davidson, K., Ishibashi, K., & Gull, T. 2001, *ApJ*, 553, 837
 Ishibashi, K., Corcoran, M. F., Davidson, *et al.* 1999, *ApJ*, 524, 983
 Okazaki, A. T., Bate, M. R., Ogilvie, G. I., & Pringle, J. E. 2002, *MNRAS*, 337, 967
 Okazaki, A. T., Owocki, S. P., Russell, C. M. P., & Corcoran, M. F. 2008, *MNRAS*, in press

Discussion

DAVIDSON: Four essential points.

(a) One cannot derive useful orbit parameters for this object from Doppler velocities, because *every* available spectral feature evolves in a complex way. Eccentricity 0.9 is possible but not established.

(b) Several years ago, Kazunori Ishibashi proposed an orbit orientation based on the X-rays. It roughly matched the parameters you adopted.

(c) η Car's spectroscopic events are *not* primarily eclipses, not even eclipses by the wind. He II, He I, near IR, photometry, and X-ray flares all show that something *far* more interesting is involved. See Martin *et al.* (2006, *ApJ* 640, 474) and references therein.

(d) The wind-wind collision region is at low latitudes but nearly all of the primary wind is polar (except during an event!).

KUDRITZKI: The X-ray dip is not an eclipse in the classical stellar sense, but rather a "wind eclipse" or an interval when the X-ray emission from the wind-wind collision is embedded in the dense wind from the primary.

OKAZAKI: Studying the effect of such an asymmetry in the primary wind on the interaction geometry is interesting. It is easy to implement the wind asymmetry in my code.